Overlap of Cu 3*d* and F 2*p* orbitals and low-energy excitations in $KCuF_3$ studied by polarization-dependent x-ray absorption and emission spectroscopy

F. Bondino,[1,*] M. Malvestuto,[2] E. Magnano,[1] M. Zangrando,[1] M. Zacchigna,[1] P. Ghigna,[3] and F. Parmigiani[1,4]
[1]*CNR-INFM, Laboratorio Nazionale TASC, Basovizza-Trieste, I-34012 Italy*
[2]*Sincrotrone Trieste S.C.p.A., Basovizza-Trieste, I-34012 Italy*
[3]*Dipartimento di Chimica Fisica "M. Rolla," Università di Pavia, V.le Taramelli 16, I-27100 Pavia, Italy*
[4]*Dipartimento di Fisica, Università degli Studi di Trieste, I-34124 Trieste, Italy*
(Received 5 September 2008; revised manuscript received 28 January 2009; published 20 March 2009; corrected 24 March 2009)

Site-, elemental-, and orbital-resolved partial density of states in $KCuF_3$ single crystal have been obtained by polarization-dependent x-ray absorption and emission spectroscopy measurements across the F *K*-edge and *ab initio* full-multiple-scattering cluster calculations. The F *K* x-ray absorption spectroscopy spectra show well-defined polarization dependence. The measurements reveal strong overlap between Cu 3*d* and F 2*p* states and identify clearly the F $2p_z$ and F $2p_{x,y}$ empty states created at different F sites. The calculations, performed for the nonequivalent F sites in the structure, confirm the energy overlap, the charge transfer between Cu 3*d* and F 2*p* states, and the different F 2*p*-Cu 3*d* overlap for the two nonequivalent F sites of $KCuF_3$. Across the F *K* edge, resonant x-ray emission spectroscopy detects a broad peak due to *d*-*d* excitations centered at about 1.2–1.6 eV and an intense charge-transfer-like transition around 7 eV.

DOI: 10.1103/PhysRevB.79.115120 PACS number(s): 71.20.−b, 78.70.Dm, 78.70.En

I. INTRODUCTION

$KCuF_3$ is an insulator that crystallizes at room temperature in a pseudocubic perovskite with distorted CuF_6 octhaedra. The cooperative Jahn-Teller effect causes the fluorine atoms to move off the midposition between two neighboring Cu atoms in the (100) plane (*ab* plane).[1] The crystal structure contains two nonequivalent fluorine atoms, which will be denoted as F_1 and F_2 (Fig. 1). F_2 sites with an asymmetric Cu-F_2-Cu bond form a long and a short Cu-F_2 bond in the *ab* plane, with Cu-F distances d_l=2.253 Å and d_s=1.888 Å, respectively. F_1 sites form symmetrical Cu-F_1-Cu bonds of intermediate Cu-F distance d_m=1.962 Å along the *c* axis.[2] Two distinct types of polytype structures occur naturally in $KCuF_3$ and usually coexist. In the type *a* (twisted), the direction of the displacement of F ions from the midpoint of adjacent Cu sites is opposite in neighboring *ab* planes, whereas in the type *d* (untwisted) the displacements are of F ions always in the same sense in neighboring *ab* planes.

The system exhibits low-dimensional magnetic properties equivalent to a nearly one-dimensional (1D) Heisenberg spin system with strongly anisotropic exchange interactions, which are much weaker in the *ab* plane than along the *c* axis.[3,4] Below 38 K (for type *a*) and 22 K (for type *d*), a three-dimensional antiferromagnetic (AF) magnetic order develops along the *c* axis.[5] The proposal that magnetic order can be driven by orbital ordering has stimulated great interest and many investigations. These investigations have been mainly based on Cu *K*-edge resonant x-ray scattering (RXS) experiments, where, however, it is challenging to disentangle the influence of the lattice distortion from that of the 3*d* orbital order itself.[6–9] The divalent copper ion in $KCuF_3$ has theoretically a d^9 configuration, which should be $t_{2g}\uparrow^3$, $t_{2g}\downarrow^3$, $e_g\uparrow^2$, $e_g\downarrow^1$ in an octahedral symmetry. However, concomitant to the orbital ordering, a cooperative Jahn-Teller distortion takes place[10] and lifts the degeneracy of the e_g orbitals, leading to an orbital ordering with an alternate occupation of $3dx^2$-z^2 and $3dy^2$-z^2 hole orbitals along the *a* and *b* crystallographic directions. This orbital ordering is set in well above room temperature.[6,7]

An interesting issue is the Cu-F bond. The strong electronegativity of fluorine is believed to give rise to a marked ionic bond with the e_g hole almost entirely localized on the Cu ion. However, the possible presence of overlap between Cu magnetic ions and F ligand ions can play an important role in the magnetism, orbital order phenomena, and Jahn-Teller distortions of the CuF_6 octahedra and cannot be neglected in the theoretical models. In a recent measurement of Cu L_{32} x-ray absorption spectroscopy (XAS) (Ref. 11) and calculations,[4] a significant ionic character of the Cu^{2+}-F bond was suggested, with net atomic charges close to their formal values. On the other hand, the differential charge-density maps for $KCuF_3$ calculated by Binggeli and Altarelli[8] indicate a significant interaction between Cu 3*d* e_g and F 2*p* states and a related non-negligible delocalization of the Cu hole on the nearest-neighbor F 2*p* states. Furthermore, an analysis of the Cu *K*-edge XAS line shape suggests that in the ground state, besides the $3d^9$ configuration with the hole localized on the Cu ion, there is also a $3d^{10}\underline{L}$ ground state configuration with a 2*p* ligand hole in the fluorine atom.[12] A direct experimental probe of F 2*p*-Cu 3*d* interaction could help to clarify this point.

A direct measurement of the orbital overlap between metal 3*d* with ligand *p* states can be provided by polarization-dependent inner-shell measurements, such as XAS and x-ray emission spectroscopy (XES) at the F *K* edge. In principle, these complementary measurements can give valuable information about the local character and orbital distribution in the F 2*p* conduction and valence bands.

In this paper we report the results of a combined theoretical and experimental investigation on $KCuF_3$ single crystal. The experiment exploited the polarization dependence of bulk-sensitive F *K* fluorescence-yield x-ray absorption and emission spectroscopy to probe directly the local F 2*p* unoc-

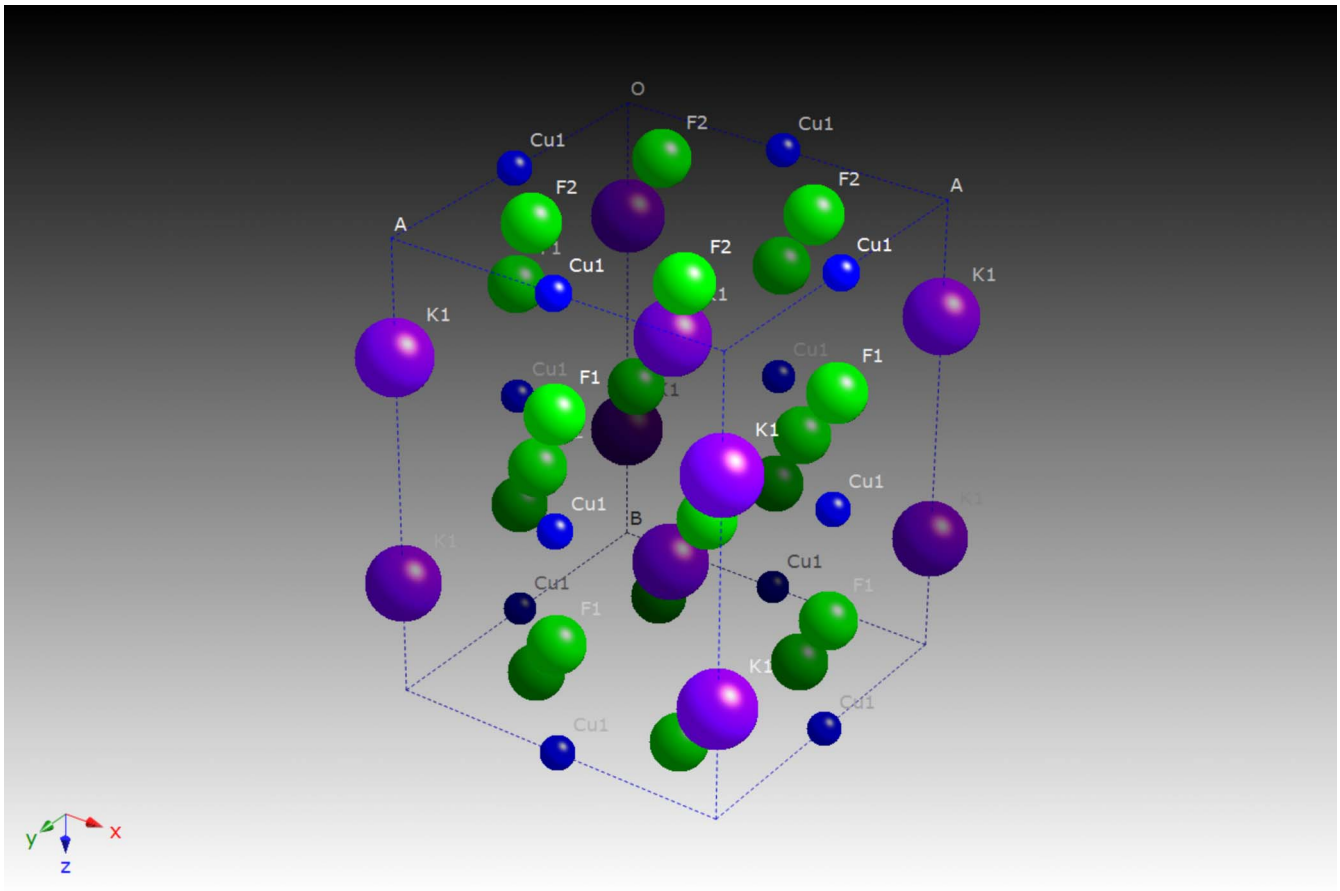

FIG. 1. (Color online) Unit cell of $KCuF_3$ at room temperature representing first nearest neighborhood (atoms K_1 and Cu_1) of the fluorine ion (F) located at the nonequivalent site F_1 and nearest neighborhood (atoms K_2 and Cu_2) of the fluorine ion located at the nonequivalent site F_2.

cupied and occupied density of states (DOS), respectively. Polarized light was used to detect the different overlap of the nonequivalent F sites in the single crystal. We have also investigated the resonant behavior of XES at F *K* edge in order to detect possible excitations across the band gap. All experimental features can be explained by the comparison with symmetry-resolved partial DOS calculations, which have been performed for this system using an *ab initio* full-multiple-scattering (FMS) approach.

II. EXPERIMENT

The measurements were performed on a $KCuF_3$ single crystal of transparent pale-violet color with a surface of about 5×3 mm^2 and thickness of about 1 mm. The crystal was cut along the (110) surface plane containing the [001] and the [110] directions.

All the measurements were performed at the BACH beamline of the Elettra synchrotron facility in Trieste.[13,14] The XAS data were acquired in total fluorescence yield (FY) using a silicon photodiode. The sample was mounted vertically, with the *c* axis ([001]) in the horizontal plane. The possibility to select either horizontal or vertical linear polarization of the incident light allows an accurate polarization study without introducing geometry factors due to different optical paths in the process. Alternatively, the absorption geometry could be varied by rotating the sample around the polar angle from normal to grazing incidence. The monochromator energy resolution was set to 300 meV at the F *K* edge. The presence of oxygen in the bulk of the sample was excluded by FY O *K* XAS and O K_α XES measurements. The incident photon energies were calibrated by measuring the Au $4f_{7/2}$ photoelectron core level with a VSW 150-mm electron analyzer during the same experiment.

Normal and resonant XES measurements were acquired with a grating fluorescence spectrometer[15] mounted in the horizontal plane at 60° from the incident photon beam. For this set of measurements the combined resolving power of the beamline and the spectrometer monochromators was around 800 at the second diffraction order. The scattering geometry was changed from nearly depolarized to polarized geometry, i.e., using linear-horizontal and linear-vertical incident-light polarization, respectively. All the measurements have been performed at room temperature.

III. COMPUTATIONS

The F *K* XAS and F K_α XES data have been modeled using an *ab initio* FMS approach implemented in the FEFF 8.4 code (as described in Ref. 16). The $KCuF_3$ crystal structure

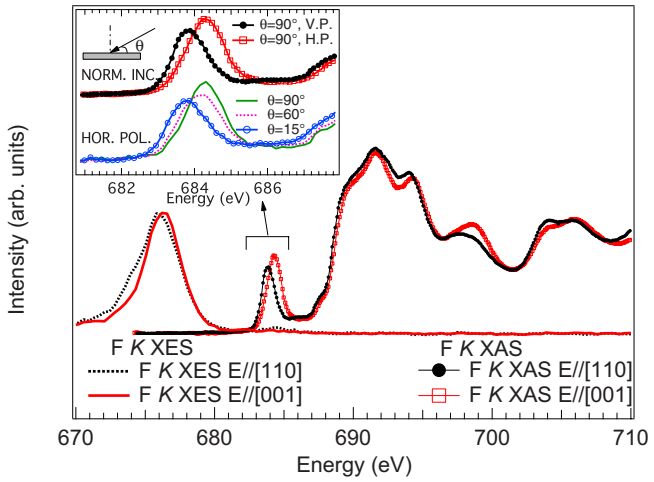

FIG. 2. (Color online) Main panel: F *K* XES and XAS spectra from $KCuF_3$ measured at room temperature, at normal incidence (θ=90°) for the $E\|[001]$ (*c* axis) and $E\|[110]$, using horizontal polarization (HP) and vertical polarization (VP), respectively. The F *K* XES spectra have been acquired with excitation energy of 684.3 eV. Inset: enlarged view of the F *K* XAS prepeak. The top curves are measured without changing the absorption geometry, at fixed photon incidence (θ=90°), as a function of the direction of linear light polarization *E* from HP ($E\|c$ *axis*) to VP ($E\|[110]$); the bottom curves are a different set of measurements obtained using fixed light polarization (HP), as a function of the incidence angle (θ). θ=90° corresponds to $E\|c$ *axis*, θ=15° corresponds to *E* almost parallel to [110] crystallographic direction.

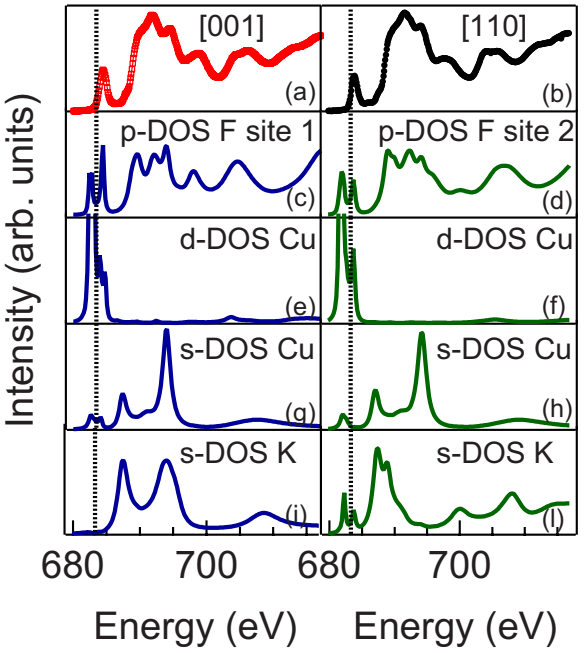

FIG. 3. (Color online) Experimental polarization-dependent F *K* XAS spectra for the $E\|[001]$ (*c* axis) and $E\|[110]$ [panels (a) and (b)] compared to the polarization-dependent partial-density-of-states calculations performed along the [001] and [110] (*c* axis) crystallographic directions for the [panels (c) to (l)] F_1 and F_2 fluorine sites, respectively.

resolved by means of x-ray diffraction analysis[2] was used as an input to the XAS calculations.

The simulations were performed using two atomic cluster models centered on the two nonequivalent sites occupied by the F ions (F_1 and F_2) in the type-*a* $KCuF_3$ crystal structure; the nonequivalence consists of different local atomic surroundings for the two F sites as apparent in Fig. 1. Model clusters consist of 221 atoms (i.e., seven coordination shells around the central F). A self–consistency radius (4.2 Å) was chosen in order to include all the first and second coordination shell atoms, while the FMS radius was fixed to 8 Å to include all atoms in the cluster. The polarization-dependent calculations were performed along the [110] and [001] (*c* axis) crystallographic directions. An overall rigid energy shift of the calculated data was required to account for the energy mismatch between the experimental F *K* XAS and calculated F *K* edge position. Calculations have been repeated for the polytype-*d* crystal structure. No significant differences are found at the energy scale of our experiment in the electronic structures obtained for the two different polytypes.

IV. RESULTS AND DISCUSSION

A. F *K* x-ray absorption spectroscopy

The F *K* XAS recorded with the light polarization *E* oriented along the [001] and [110] crystallographic directions of $KCuF_3$ are reported in Fig. 2. In order to suppress saturation-derived effects in the comparison of the spectra, the data have been collected without changing the absorption geometry, at fixed photon incidence, by changing the direction of linear light polarization *E* from horizontal ($E\|c$ *axis*) to vertical ($E\|[110]$). The same qualitative behavior has been observed by changing the incidence polar angle (see inset of Fig. 2).

The line shape of these spectra is clearly different from those of the alkali-metal fluorides without localized *d* electrons such as KF.[17] The most striking difference is the presence in $KCuF_3$ of a pre-threshold peak around 684 eV. A similar prepeak was detected in other copper fluorides such as in K_2CuF_4 (Ref. 18) and CuF_2,[19] where transition 3*d* states are mixed with the ligand 2*p* states in the conduction band.

These qualitative observations indicate that the pre-threshold peak in $KCuF_3$ is directly related to an admixture of Cu 3*d* and F 2*p* orbitals in the ground state. This empirical assignment is supported by the partial-density-of-states calculations reported in Fig. 3, which find an overlap of F 2*p* and Cu 3*d*-e_g empty states at the onset of x-ray absorption.

In a pure ionic picture the fluorine 2*p* shell should be full. However, both the F *K* XAS and the calculations indicate that empty F 2*p* holes are likely created favored by the ground-state overlap between Cu 3*d* and F 2*p* orbitals. The orbital occupation numbers derived from the calculations and reported in Table I are in agreement with this picture. Although some precautions have to be taken in the interpretation of these data since the calculated occupation numbers depend to some extent on the choice of the atomic radii of

TABLE I. Calculated orbital occupation numbers for the different shells of the elements located at different sites of $KCuF_3$ (the sites are described in Fig. 1). Some precautions have to be taken in the interpretation of these data since the calculated occupation numbers depend to some extent on the choice of the atomic radii of the muffin-tin spheres.

	s	*p*	*d*
F_1	1.983	5.693	
F_2	1.980	5.706	
Cu_1	0.415	0.491	9.751
Cu_2	0.392	0.478	9.786
K_1	0.660		
K_2	0.664		

the muffin-tin spheres, the results show that the F $2p$ shell, with ~5.7 electrons per atom, is not full and the extra charge is localized on the K $4s$ and Cu $3d$ states, with ~9.7 electrons per Cu atom, in contrast with a pure ionic picture Cu $3d^9$ F $2p^6$.

Due to the dipole selection rules, the absorption coefficients for the $E\|c$ and $E\|[110]$ geometries reflect the F $2p_z$ (out-of-plane) and F $2p_{x,y}$ (in-plane) character hole states, respectively. Owing to the site selectivity of polarized x-ray absorption and the crystal structure of $KCuF_3$, these two experimental configurations, $E\|c$ and $E\|[110]$, selectively probe F-Cu bonds of the two different F sites. In particular, the configuration with $E\|c$ detects the F $2p_z$ orbitals of the F_1 site hybridized with the Cu $3d_{(z2\text{-}x2)/(z2\text{-}y2)}$ unoccupied orbitals, while the configuration with $E\|[110]$ corresponds to the F $2p_{x,y}$ holes of the F_2 site overlapped with Cu $3d_{(z2\text{-}x2)/(z2\text{-}y2)}$ holes. Experimentally, the F K XAS spectra show a well-defined polarization and geometry dependence. The prepeak shifts in energy and appears at 0.5 eV lower absorption energy when the linear polarization orientation is changed from the c axis to the [110] direction. Therefore, according the previous arguments, the lower-energy prepeak in the experimental F K XAS obtained when $E\|[110]$ should correspond to F_2 $2p_{x,y}$ states, while the higher-energy prepeak obtained when $E\|c$ should correspond to F_1 $2p_z$ holes.

This is precisely what is obtained from our calculations, which therefore confirm this assignment. Indeed, calculations find the F p DOS of two nonequivalent F_1 and F_2 sites of $KCuF_3$ at different energies, with the F_2 prepeak at lower energy with respect to the F_1 prepeak.

The F p-projected density of states, Cu d- and s-projected DOS, and K s-projected DOSs calculated using atomic cluster models centered on the two nonequivalent F_1 and F_2 sites are reported in Fig. 3 and compared with the experimental XAS F K-edge data acquired with $E\|[001]$ and $E\|[110]$. By associating the projected DOSs of each photoelectron scattering site that contribute to individual features in the calculated spectrum (Fig. 3), a detailed understanding of the K edge XAS is obtained. The predicted F p DOS agrees with the experiment, reproducing well all the main features of the measured spectra on the overall energy range considered. The overall line shapes of the p-DOSs calculated for the F_1 and F_2 sites appear to be slightly different because of the nonequivalent F ion sites.

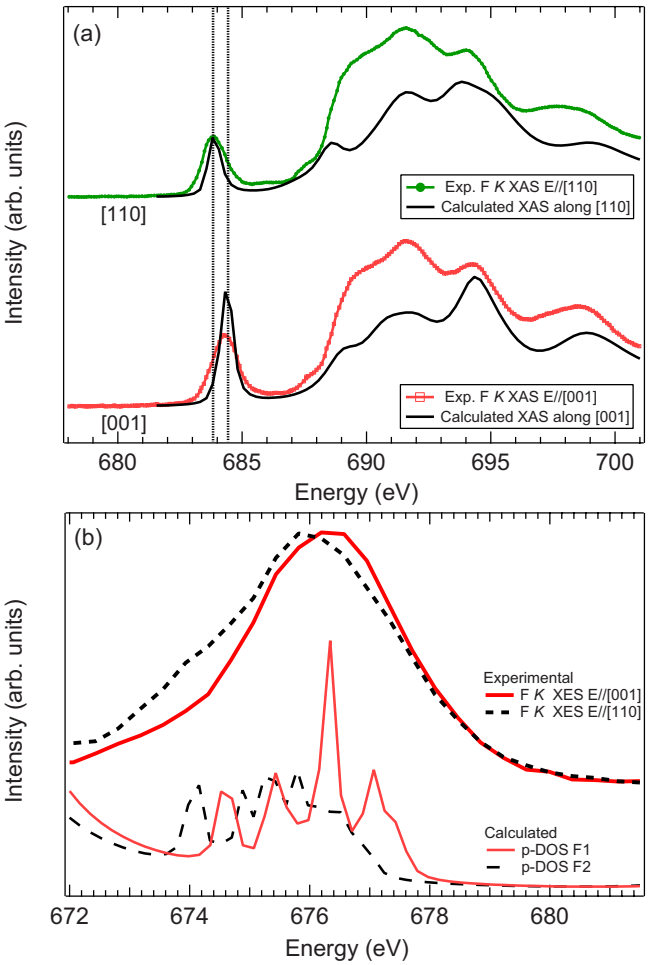

FIG. 4. (Color online) (a) Polarization-dependent XAS spectra calculated for the polarization vector along the [001] and [110] crystallographic directions for the F_1 and F_2 fluorine sites compared to the experimental polarization-dependent F K XAS spectra. The same energy shift observed in the experimental F K XAS prepeak is also obtained in the calculations. (b) Polarization-dependent XES spectra compared to the partial DOS calculated for the F_1 and F_2 sites. The same shift has been applied to the partial F $2p$ DOS in order to align them on the experimental data.

The experimental F K XAS is reported in Fig. 4(a) in comparison with the calculated F K XAS for the F_1 and F_2 sites for the $E\|[001]$ and $E\|[110]$ light polarizations, respectively. Interestingly, the relative positions of the pre-edge region of the simulated p-DOSs display an energy shift like the experiment. The calculated XAS spectra in Fig. 4 find that a pre-edge peak for the F_1 ion site is present when light polarization E is parallel to the c axis, while no pre-edge peak is present when E is perpendicular to the c axis. The exact opposite situation occurs in the case of the F_2 site [see Fig. 4(a)]. The experimental energy positions of the XAS pre-edge peak upon the two different polarization directions are well reproduced by the calculation. These findings provide strong evidence that the pre-edge peak energy position is sensitive to the nonequivalence of the F ion sites scanned through the polarization orbital selection rules.

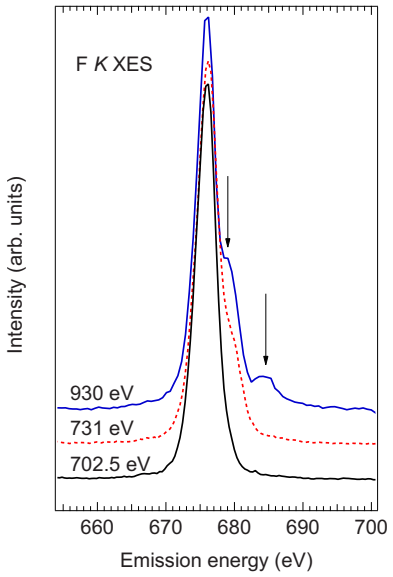

FIG. 5. (Color online) F *K* XES spectra measured from $KCuF_3$ at different excitation energies. The spectra have been normalized at the same intensity. The high-energy satellites are marked with arrows.

B. F *K* x-ray emission and resonant x-ray emission spectroscopy

F *K* XES measurements have been performed for excitation energies ranging from 681.7 eV (which is just below the F *K* XAS prepeak) to 945 eV (which is ~260 eV above the threshold). For excitation energies below the F *K* XAS prepeak we have found a resonant regime, where it was possible to observe spectral features at constant energy loss from the elastic peak. For excitation energies equal to and above the F *K* XAS prepeak, but still close to the F *K* threshold, we have found a normal fluorescencelike regime with the spectral features appearing at constant emission energy. For energies well above the F *K* threshold, two well-defined high-energy emission satellites appear in the F *K* XES spectra.

Due to dipole selection rules, the F *K* x-ray emission is produced during the transition of 2*p* electrons of the valence band to the 1*s* core hole. In the normal fluorescence regime, observed for excitation energies between 682.3 and 700 eV, the F *K* emission is found at constant emission energy and it can be then regarded as an experimental probe of fluorine *p* partial density of states as discussed in detail by Anisimov *et al.*[20] Using the elastic peak as a reference for energy calibration, the F *K* XES spectra can be plotted together with the F *K* XAS, obtaining an experimental determination of partial (F 2*p*) empty and occupied DOS, respectively. This peak appears to be sensitive to the orientation of the electrical polarization with respect to the crystallographic directions. It shows a broadening when the orientation is changed from the *c* axis to the [110] axis (Fig. 2). This broadening can be explained by the different energy extension of F 2*p* density of states of the two nonequivalent F_1 and F_2 sites as shown by the calculations reported in Fig. 4(b).

For excitation energies well above the F 1*s* ionization threshold, for instance for $h\nu=731$ eV or $h\nu=930$ eV which are ~50 and ~250 eV above the threshold, respectively, the F K_α XES spectra show strong high-emission energy satellites as can be observed in Fig. 5. These satellites are absent for excitation energies set on or just above the F *K* absorption edge, e.g., at 702.5 eV and below this energy. Figure 5 shows that at 731 eV a first structure appears at emission energy of ~679 eV, at ~3 eV above the main emission line. At 930 eV, a further satellite at ~684.6 eV, which is ~9 eV above the main emission line, is also visible. These satellites have been already observed in many fluorides, such as in NaF, MgF_2, PbF_2, CuF_2, Na_3AlF_6,[21] LiF,[22] K_2TiF_6, FeF_3, FeF_2,[23] and CuF_2,[24] and they have been explained as to be originated from ionized states in the F *L* shell, i.e., interatomic electronic transitions occurring prior to K_α emission in the presence of one or two further spectator holes in the *L* shell.[25–27] The first satellite with an energy shift ~3 eV from the main F $K\alpha$ line is originated from one spectator hole in the 2*p* shell and it has a complex energy dependence.[26,27] The higher-energy satellite is originated from an initial configuration with a single *K* shell vacancy and a double *L* shell vacancy and starts to be visible above 750 eV[26] due to the higher onset of this triple-vacancy excitation.

In the resonant regime, the excitation energy dependence of the RXES spectra allows the identification of two resonant inelastic x-ray-scattering (RIXS) structures, i.e., emission peaks, which do not appear at constant emission energy, but at constant energy loss from the elastic peak. This Raman-type linear dispersion of x-ray emission peak is observed in the subthreshold region for excitation energies set below the copper-fluorine prepeak of the F *K* XAS. The energy loss can be qualitatively interpreted as energy lost by the system during the resonant RXES process for low-energy excitations. Figure 6(a) shows the F *K* XES spectra measured at different orientations of the light polarization with respect to the crystal axis. In these spectra the electrical vector has been changed from along the *c* axis (0°) toward the [110] orientation in steps of 30°. The spectra show a clear RIXS peak (labeled A in Fig. 6) with energy loss in a range between 1.2 and 1.6 eV. This RIXS peak is detected at constant energy loss from the elastic peak (labeled E in Fig. 6) for each orientation of the incident polarization for excitation energies below the F *K* prepeak. For higher excitation energies this component disappears. A second peak is also detected, in a very narrow energy range of excitation energies below F *K* prepeak, at ~7.3 eV constant energy loss from the elastic peak E for each orientation of the incident polarization for excitation energies well below the F *K* prepeak. For higher excitation energies this peak is converted in a normal fluorescence line at constant emission energy, which can be associated to F 2*p* partial density of states as discussed previously.

The resonant behavior of these peaks and the comparison with the semiempirical LDA+*U* calculations[8] provide a possible interpretation of the observed transitions. The observed RIXS peaks can be interpreted as electronic excitations between the occupied and the empty states. In particular, the broad low-energy peak at 1.2÷1.6 eV may correspond to *dd* transitions which are likely to be an overlap of several crystal-field peaks, unresolved in the present experiment. This interpretation is supported by recent optical

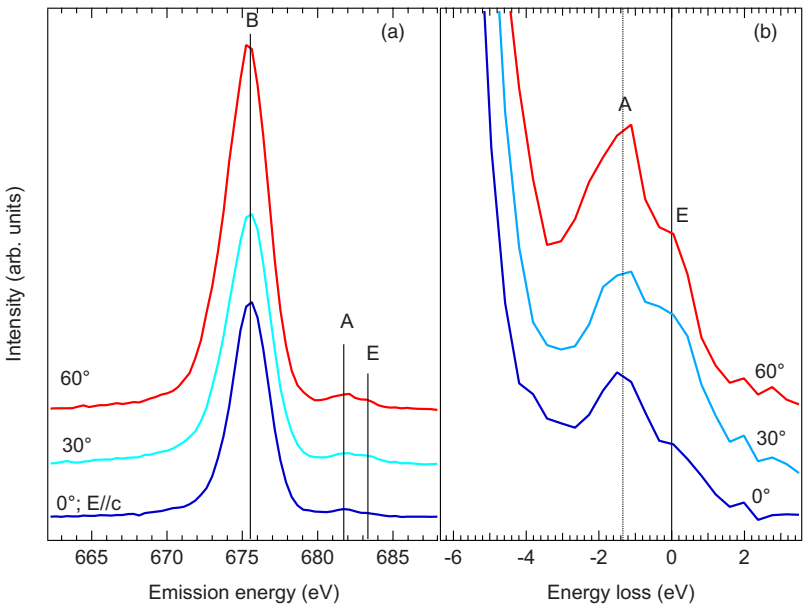

FIG. 6. (Color online) F *K* RXES measured at 683.3 eV with linear-horizontal polarization at different incidence angles from $E\|c$ axis (0°) toward the [110] direction (90°) in steps of 30°. (a) F *K* RXES spectra in the emission energy scale. E, A, B indicate the elastic peak, and the RIXS components A and B respectively. (b) Enlarged view of the region close to the elastic peak in an energy-loss scale, with the elastic peaks set at 0 eV.

measurements.[28] For excitation energies on the leading edge of the F *K* prepeak the peak detected at ~7 eV constant energy loss from the elastic peak can be interpreted as a charge-transfer transition from the F 2*p*-Cu 3*d* admixed states to the empty Cu 3*d* states. The interpretation is supported by the fact that these RIXS peaks are only observed for excitation energies set on the F *K* XAS prepeak, which is mainly originated by Cu 3*d* states overlapped with F 2*p* orbitals.

V. CONCLUSIONS

Elemental- and orbital-resolved $KCuF_3$ valence and conduction bands have been measured by x-ray absorption and emission spectroscopy and calculated by *ab initio* multiple-scattering cluster formalism. F *K*-edge XAS displays a clear absorption pre-threshold peak, arising from Cu 3*d*-F 2*p* overlapped orbitals, whose position shifts by about 0.5 eV to higher energy when the light linear polarization is rotated from the [110] to the [001] crystallographic directions. The marked polarization dependence of F 2*p* XAS prepeak is due to the different energy overlap of Cu 3*d* states and F 2*p* orbitals at the different fluorine sites. The results support the presence of a partial covalent admixture of Cu 3*d* and F 2*p* states, in contrast with a picture of a significant ionic Cu^{2+}-F bond.

This covalent Cu 3*d*-F 2*p* admixture allows the observation of Cu-related low-energy RIXS excitations at F *K* edge (in particular for selective energy excitation on the F *K* XAS prepeak). These excitations detected on the leading edge of the F *K* XAS prepeak can be interpreted as Cu *d*-*d* and F 2*p*-Cu 3*d* charge-transfer transitions.

ACKNOWLEDGMENTS

F.B. acknowledges J. Deisenhofer for useful discussions.

*Corresponding author. bondino@tasc.infm.it

[1] J. Kanamori, J. Appl. Phys. **31**, S14 (1960).
[2] R. H. Buttner, E. N. Maslen, and N. Spadaccini, Acta Crystallogr. B **46**, 131 (1990).
[3] M. T. Hutchings, H. Ikeda, and J. M. Milne, J. Phys. C **12**, L739 (1979).
[4] M. D. Towler, R. Dovesi, and V. R. Saunders, Phys. Rev. B **52**, 10150 (1995).
[5] M. T. Hutchings, E. J. Samuelse, G. Shirane, and K. Hirakawa, Phys. Rev. **188**, 919 (1969).
[6] L. Paolasini, R. Caciuffo, A. Sollier, P. Ghigna, and M. Altarelli, Phys. Rev. Lett. **88**, 106403 (2002).
[7] R. Caciuffo, L. Paolasini, A. Sollier, P. Ghigna, E. Pavarini, J. van den Brink, and M. Altarelli, Phys. Rev. B **65**, 174425 (2002).
[8] N. Binggeli and M. Altarelli, Phys. Rev. B **70**, 085117 (2004).
[9] M. Takahashi, M. Usuda, and J. I. Igarashi, Phys. Rev. B **67**, 064425 (2003).
[10] K. I. Kugel and D. I. Khomskii, Usp. Fiz. Nauk **136**, 621 (1982) [Sov. Phys. Usp. **25**, 231 (1982)].
[11] C. De Nadaï, A. Demourgues, J. Grannec, and F. M. F. de Groot, Phys. Rev. B **63**, 125123 (2001).
[12] J. Chaboy, A. Muñoz-Páez, and E. Sánchez Marcos, J. Synchrotron Radiat. **13**, 471 (2006).
[13] M. Zangrando, M. Finazzi, G. Paolucci, G. Comelli, B. Diviacco, R. P. Walker, D. Cocco, and F. Parmigiani, Rev. Sci. Instrum. **72**, 1313 (2001).
[14] M. Zangrando, M. Zacchigna, M. Finazzi, D. Cocco, R. Rochow, and F. Parmigiani, Rev. Sci. Instrum. **75**, 31 (2004).
[15] D. Cocco, M. Zangrando, M. Matteucci, F. Bondino, M. Platè, M. Zacchigna, F. Parmigiani, B. Nelles, and K. C. Prince, AIP Conf. Proc. **705**, 873 (2004).

[16] A. L. Ankudinov, B. Ravel, J. J. Rehr, and S. D. Conradson, Phys. Rev. B **58**, 7565 (1998).
[17] E. L. Shirley, Phys. Rev. Lett. **80**, 794 (1998).
[18] H. Manaka, T. Koide, T. Shidara, and I. Yamada, Phys. Rev. B **68**, 184412 (2003).
[19] S. Nakai, A. Kawata, M. Ohashi, M. Kitamura, C. Sugiura, T. Mitsuishi, and H. Maezawa, Phys. Rev. B **37**, 10895 (1988).
[20] V. I. Anisimov, P. Kuiper, and J. Nordgren, Phys. Rev. B **50**, 8257 (1994).
[21] H. Endo, M. Uda, and K. Maeda, Phys. Rev. A **22**, 1436 (1980).
[22] A. Kikas, T. Käämbre, V. Kisand, A. Saar, K. Kooser, E. Nõmmiste, and I. Martinson, J. Electron Spectrosc. Relat. Phenom. **144-147**, 845 (2005).
[23] S. A. Krasnikov, A. S. Vinogradov, A. B. Preobrajenski, L. K. Gridneva, S. L. Molodtsov, C. Laubschat, and R. Szargan, Phys. Scr. **T115**, 1074 (2005).
[24] S. M. Butorin, V. R. Galakhov, E. Z. Kurmaev, S. M. Cheshnitsky, S. A. Lebedev, and E. F. Kukovitzkii, Phys. Rev. B **47**, 9035 (1993).
[25] E. H. Kennard and E. Ramberg, Phys. Rev. **46**, 1040 (1934).
[26] M. Oura, T. Mukoyama, M. Taguchi, T. Takeuchi, T. Haruna, and S. Shin, Phys. Rev. Lett. **90**, 173002 (2003).
[27] J.-E. Rubensson, S. Eisebitt, M. Nicodemus, T. Böske, and W. Eberhardt, Phys. Rev. B **50**, 9035 (1994).
[28] J. Deisenhofer, I. Leonov, M. V. Eremin, Ch. Kant, P. Ghigna, F. Mayr, V. V. Iglamov, V. I. Anisimov, and D. van der Marel, Phys. Rev. Lett. **101**, 157406 (2008).